Journal of Computer-Aided Molecular Design (2022) 36:279–289
https://doi.org/10.1007/s10822-022-00451-8

Role of water coordination at zinc binding site and its catalytic pathway of dizinc creatininase: insights from quantum cluster approach

Wijitra Meelua[1,2] · Julianna Oláh[3] · Jitrayut Jitonnom[2]

Received: 1 December 2021 / Accepted: 17 March 2022 / Published online: 6 April 2022

Abstract
Creatininase is a key enzyme of creatinine-metabolizing pathway in mammals, and has a great potential for diagnostic application. It catalyzes the reversible conversion of creatinine to creatine. Here, we investigated its reaction mechanism with density functional theory in conjunction with the quantum cluster approach. Three reaction pathways in which several possible proton transfers assisted by either His178 or a water ligand to Zn1 (Wat2) or both were considered. DFT calculations reveal, depending on Wat2 coordination mode at Zn1, two competitive ring-opening pathways where His178 playing a central role as a proton shuttle or both His178 and Wat2 serving as a dual catalytic role as a base and an acid, respectively. Three elementary steps were proposed for the reaction: the first involves nucleophilic attack by a bridging hydroxide to the substrate and forms a gem-diolate intermediate, followed by a proton transfer from the gem-diolate to His178 (His178 protonation is a required step for efficient proton transfers). Finally, the second proton transfer from the protonated His178 or Wat2 to the amide of substrate leads to the ring opening. The first proton transfer is the rate-limiting step of the whole reaction, in consistent with previous experimental and computational studies. A detailed understanding of the reaction mechanism of the creatininase enzyme family will also be helpful for developing a biosensor for kidney function.

Keywords Density functional theory · QM cluster approach · Creatininase · Reaction mechanism, dizinc

Introduction

Creatininase (creatinine amidohydrolase; EC 3.5.2.10), is a member of the urease-related amidohydrolase superfamily. It is a creatinine-metabolizing enzyme that catalyzes hydrolysis of creatinine to creatine, which is a breakdown product of creatine metabolism in mammals. This enzyme plays a key role in the bacterial degradation of creatinine [1] and participates in arginine and proline metabolism. In medicine, the creatininase has a great potential for diagnostic application, including its use as biosensors for accurate measurement of renal function [2]. Creatininase from *Pseudomonas putida* has been extensively studied [3–9]. Pioneering works on the structure and function of the creatininase enzyme were described by Beuth et al. and Yoshimoto et al. [10–14]. The X-ray crystal structures of creatininase in its apo and product complex forms revealed that it is a typical zinc enzyme with a binuclear metal center as a metal cofactor at the active site of each subunit (Mn^{2+}/Zn^{2+} or Zn^{2+}/Zn^{2+}) [11, 14]. The binuclear metal center is bridged by an aspartate (Asp45) and a zinc-bound water or a hydroxide ion (Wat1) (see Scheme 1). Zn1/Mn1 is liganded by three protein residues (Glu34, Asp45, and His120), a carbonyl oxygen of the creatinine substrate, and the bridging hydroxide Wat1, while Zn2 is liganded by three protein residues (His36, Asp45, and Glu183) and Wat1. In the active site, there is a second water molecule (Wat2) situated very close to Zn1 and the

✉ Jitrayut Jitonnom
jitrayut.018@gmail.com

[1] Demonstration School University of Phayao, 56000 Phayao, Thailand

[2] Division of Chemistry, School of Science, University of Phayao, 56000 Phayao, Thailand

[3] Department of Inorganic and Analytical Chemistry, Budapest University of Technology and Economics, Gellért tér 4, H-1111 Budapest, Hungary

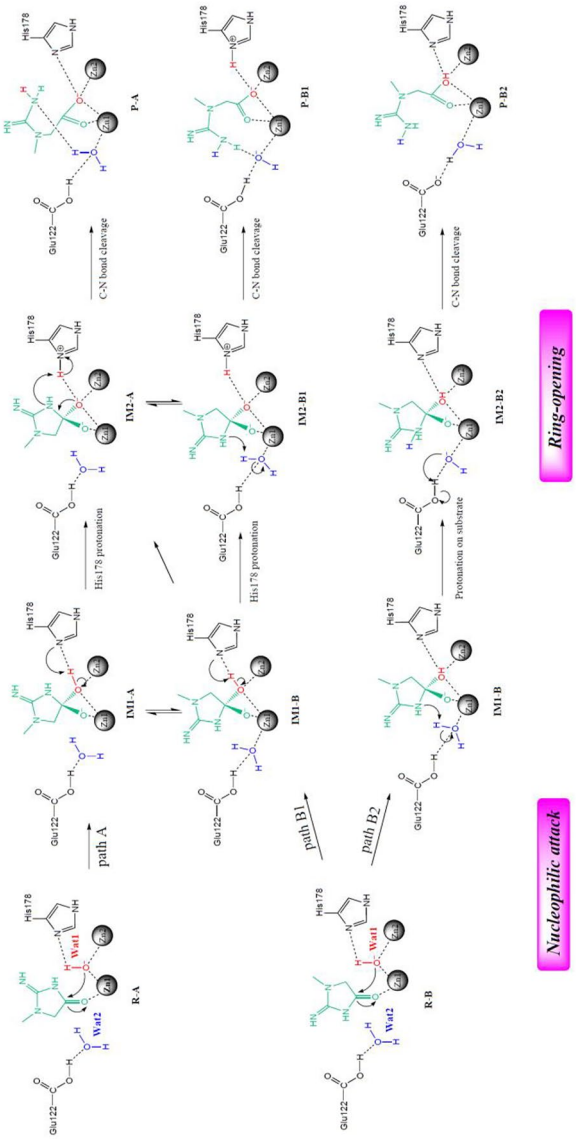

Scheme 1 Possible reaction pathways (paths A, B1 and B2) considered in this study. Path A refers to the His178-assisted mechanism (via protonated His178) suggested by Beuth et al. [11] and Jitonnom et al. [15], while path B involved the water-assisted mechanism proposed by Yoshimoto et al. [13, 14] where the active site water, Wat2, nearby Glu122 and Zn1 acts as a proton donor of the ring-opening step if His178 is protonated or unprotonated (referred to paths B1 and B2, respectively)

Glu122 residue, which belongs to the second-shell. Mutational and computational studies [13, 15] suggest that the lack of Glu122-Wat2 interaction in the Glu122Asn mutant accounts for the reduced activity.

Similarly to other dinuclear zinc enzymes ([16–21], the reaction mechanism of creatininase occurs via nucleophilic attack and ring opening. The first step is quite common to in these zinc metalloenzymes, i.e., the bridging water performs a nucleophilic attack on the substrate carbonyl carbon, leading to the formation of tetrahedral intermediate. However, in the ring-opening step, the precise mechanism and the significant roles of the proton donor remain unclear. Several experimental and computational studies have been carried out to identify the exact proton donor of the catalytic reaction in creatininase, which was suggested to be either the His178 residue or a water molecule, Wat2, in the enzyme active site (hereafter named path A and path B, respectively; Scheme 1). In a proposed mechanism suggested by Beuth et al. [11] (path A in Scheme 1), the bridging hydroxide Wat1 acts as the nucleophile in the first nucleophilic attack step, whereas the His178 serves as a proton donor in the ring-opening step. The His178Ala mutation abolished the activity of the enzymes calling the attention to the crucial role of His178 in catalysis [13]. Contrary this suggestion, Yoshimoto et al. [13, 14] (path B2 in Scheme 1), proposed that instead of His178 a second water molecule Wat2 acts as a proton donor in the ring-opening step. However, our recent QM/MM free-energy simulations [15] suggest that this role of Wat2 is unlikely. In particular, our computer simulations clearly show that the most likely ring-opening step occurs through one concerted proton transfer step with His178 playing a central role as a proton shuttle. Still, several details remain unclear, such as the possible dual role of both His178 and Wat2 and the zinc coordination mode during catalysis. Alternatively, apart from path A and B2 where the proton donor is His178 or Wat2, they can participate together and performs a couple role, i.e., the His178 is firstly protonated and then Wat2 serves as a proton donor in the ring opening (see path B1 in Scheme 1). This pathway B1 was not considered in the previous QM/MM study. Particularly, we wondered whether this water molecule (Wat2) would act as a proton donor once the His178 is protonated through a proton transfer from the gem-diolate proton. Here, we considered this second water molecule and its catalytic role are elucidated. Overall, this information clearly indicates that clarifying the possible dual role of both His178 and Wat2 is worthy of investigation.

In this work, we have used a combination of the density functional theory (DFT) method and the quantum cluster approach to investigate the reaction mechanism of creatininase concerning possible pathways regarding the chemistry of zinc coordination and protonation state of active site environment. A model of the active site was designed on the basis of the crystal structure, and the stationary structures and energetics of the reaction pathways (Scheme 1) were calculated. This DFT cluster approach has previously been successfully applied to study reaction mechanism of different enzymes [17–19, 22–26]. Our cluster model calculations can discriminate different mechanisms proposed earlier (Scheme 1) and provide a computational evidence for the dual role of His178 and Wat2, which have not yet

been well described. A detailed mechanistic understanding of the enzyme will enhance current knowledge and application of an enzymatic biosensor for kidney function.

Computational methods

The model system for the active site dinuclear zinc cluster of the creatininase was constructed on the basis of a high resolution X-ray crystal structure of the enzyme-product (creatine) complex of the Mn-activated creatininase (PDB entry 1V7Z) [14]), a typical Zn^{2+} enzyme with one zinc ion replaced with Mn^{2+}. To build a dizinc enzyme cluster model (Zn-Zn enzyme), the creatinine substrate was built from the X-ray structure by manually adjusting the carbon-nitrogen bond to form the five-membered ring. One oxygen atom of creatine that is bridged with two metal centers was replaced with a hydroxide anion (OH^-), a highly reactive and unstable species [27]. The manganese ion in the active site was replaced with a zinc ion to build the Zn-Zn enzyme cluster model. Hydrogen atoms were added manually, and the amino acids were truncated so that in principle only side chains were kept in the model (see Figs. 1 and 2). Truncated bonds were saturated with hydrogen atoms. Thus, the model consists of the two zinc ions along with their ligands His36, His120, His178, Glu34, Glu122, Glu183 and the bridging carboxylated Asp45 and the hydroxide ion (Wat1). With an exception of Glu122, all Glu/Asp residues were negatively charged, while His residues were neutral. For Glu122, we assigned this residue as the neutral form according to our previous study [28]. Meanwhile, according to the electronic structures the possibility of the ionized Glu122 at the initial stage of the reaction is unlikely as this would rule out a proton transfer from Wat2 to the cyclic amide nitrogen (path B in Scheme 1), considering its potential hydrogen bonds with Wat2 and Glu34 (**Figure S1**). Additionally, the second water molecule (Wat2), which is thought to be important for catalysis [13], were also included in the model. The resulting active-site model is thus composed of 87 atoms and has a zero net charge.

Following the cluster approach [29–32], truncation atoms (C_β atoms) were fixed to their corresponding positions from the X-ray structure. The model system was then optimized at the B3LYP/6-31G(d) level, with no initial symmetry restrictions and assuming C1 point group. Frequency calculations were performed on all optimized structures to obtain zero-point energy corrections to the electronic energies, and to identify all the stationary points as minima (zero imaginary frequency) or transition states (one imaginary frequency). The atomic charge distributions were also computed at the same level of theory using Mulliken population analysis [33]. More accurate B3LYP energies were also obtained by performing single-point energy calculations on the optimized geometries using a larger 6–31 + G(d,p) basis set for all elements. Solvation effect was taken into account using the conductor-like polarized continuum model (CPCM) [34] using a dielectric constant (ε) of 4, as suggested by Himo et al. [29, 30]. It was shown that inclusion of solvent effects significantly lowers the barriers and intermediate energies compared to gas phase for path A, while they increase the barriers and relative energies for path B (see **Table S1**). Altering this dielectric constant to higher or lower value does not change significantly the overall shape of the potential energy profile (ε = 1, 4, 80; see **Figure S2**). Dispersion effects were performed with DFT-D3 program as developed by Grimme et al. [35, 36]. It is shown that both implicit solvation and dispersion have a significant and important effect in lowering the energy barrier [32, 37–39]. Final reported energies are the electronic energies with the large basis set plus corrections for zero-point energy, CPCM solvation, and dispersion in kcal/mol. All calculations were performed using Gaussian 09 program [40].

Results and discussion

To further scrutinize these previously suggested mechanisms in Scheme 1 with QM cluster calculations, we first optimized the structures for the reactant complex and the structures of the proposed intermediates and their corresponding energies were evaluated for paths A, B1 and B2. The results of the QM calculations have identified seven stationary points (**R, TS1, IM1, TS2, IM2, TS3** and **P**) in all studied pathways. The main geometric results are summarized in Table 1 and visualized in Figs. 1, 2, 3, 4 and 5. All coordinates for all important structures are given in Supporting Information. Relative energies calculated for paths A, B1 and B2 using cluster model are depicted in Fig. 6. The criteria for the ligation ability of Wat2 at Zn1 were measured by the Zn1-O_w distance, having a cut-off of < 3.00 Å for bound geometry (*Wat2_bound*) and > 3.00 Å for unbound geometry (*Wat2_unbound*).

Reactant

Initially, several structures at the reactant (**R**) and intermediate (**IM**) in both bound and unbound modes of Wat2 with respective to Zn1 (hereafter, *Wat2_bound* and *Wat2_unbound*, respectively) were built and optimized. Both geometries were successfully obtained at the intermediate (**IM1-A** and **IM1-B**, **see** Figs. 3 and 4) but only *unbound* geometries were obtained at the reactant (see **R-A** and **R-B** in Figs. 1 and 2, respectively). Attempts to generate a stable structure of *bound* reactant from the *bound* intermediate

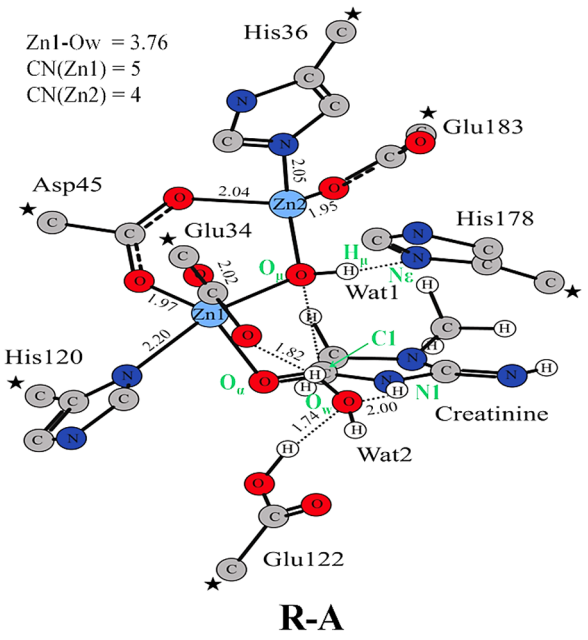

Fig. 1 DFT optimized structure of reactant for path A. For clarity, some hydrogen atoms are omitted in the figures. The fixed atoms are marked with asterisks. Distances are in angstrom (Å)

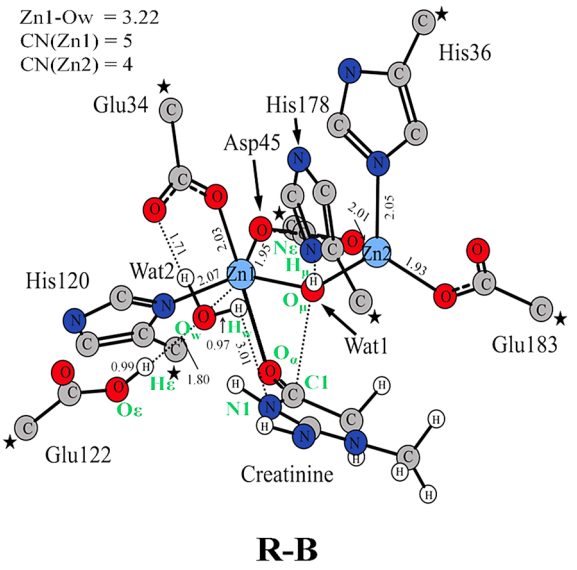

Fig. 2 DFT optimized structure of reactant for path B. For clarity, some hydrogen atoms are omitted in the figures. The fixed atoms are marked with asterisks. Distances are in angstrom (Å)

geometry (**IM1-B**) are not satisfied during the relaxed scan along the C-O distance (see **Figure S3**). Therefore, we obtained one *unbound* for the reactant, while both *bound* and *unbound* for the intermediate.

In the reactant, due to hydrogen bonding possibility of Wat2 with respect to Glu34, Glu122 and the substrate amide

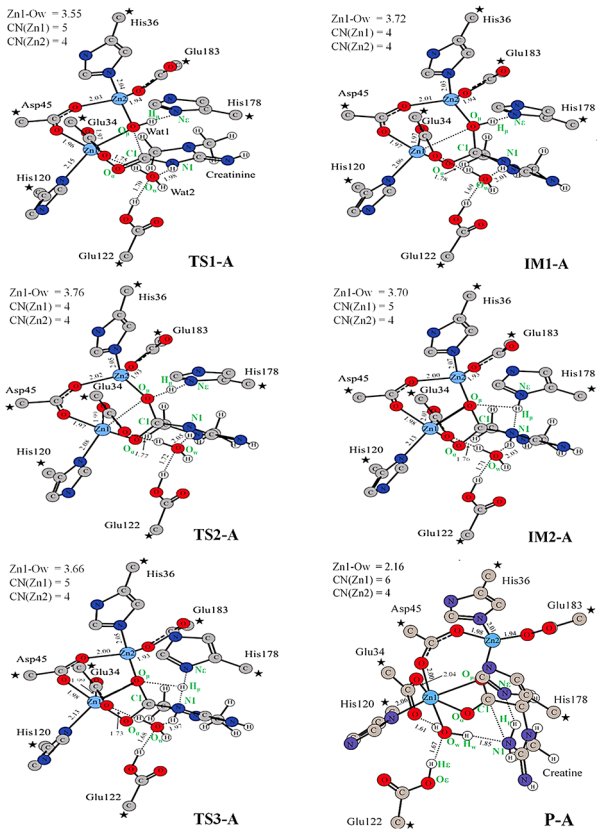

Fig. 3 DFT optimized structures of transition states, intermediates and product for path A. The fixed atoms are marked with asterisks. Distances are in angstrom (Å)

bond, this water could form, via its oxygen, a direct hydrogen bond to the substrate nitrogen atom (N1) (**R-A** in Fig. 1) or situate above the substrate prepared for a proton transfer as suggested by Yoshimoto et al. (**R-B** in Fig. 2). The optimized structure of the reactant (**R-A**) for path A is shown in Fig. 1. This structure represent the initial stage prior to the reaction to take place, which is not seen in the X-ray structure (PDB 1V7Z) [14] where the hydroxide/water was replaced by the carboxylate terminus of the creatine product. In particular, the bridging hydroxide has symmetric bonds to the two zinc ions (Zn1-O_μ = 2.03 Å and Zn2-O_μ = 1.94 Å) and forms a hydrogen bond with the His178 residue (Nε-H_μ = 1.87 Å).

The reactant structure (**R-B**) of path B is first optimized and it is shown, in Fig. 2, that the computed R-B structure is quite similar to the one calculated for path A. The minor structural difference is the orientation of Wat2 with respective to the N1 atom of substrate and the ligand coordination geometry of Zn1 (Zn1-O_w = 3.22 Å; Zn1-O_α= 2.39 Å for path B and Zn1-O_w = 3.76 Å; Zn1-O_α= 2.10 Å for path A). This Wat2 is completely unliganded to Zn1. Therefore, the coordination number is 5. With the C1-O_μ distance of 2.49 Å, the bridging hydroxide is, however, possible for in-line

nucleophilic attack, stabilized by His178 (Nε-H_μ = 1.99 Å at **R-B**). It should be mentioned that the relative energy of the reactant structure of path B (**R-B**) is by 6.5 kcal/mol more stable than that of path A (**R-A**). It is found that for both **R-A** and **R-B**, Zn1 is more electropositive than Zn2 (0.90e/0.88e on Zn1/Zn2 for path A and 0.92e/0.90e on Zn1/Zn2 for path B, **Table S2**). Similar results were also previously observed in a dizinc metallopeptidase [23].

Nucleophilic attack and ring opening

The optimized structures of transition states, intermediate and product are shown in Figs. 3, 4 and 5 and the potential energies of these stationary points calculated for all pathways are depicted in Fig. 6, with respect to the energy of the reactant **R-B**.

Path A

The first step of the reaction (Scheme 1) is a nucleophilic attack by the bridging hydroxide on the C1 atom of the substrate, leading to the formation of tetrahedral gem-diolate intermediate (**R-A→IM1-A**). This step is common to other hydrolytic dinuclear zinc enzymes [16]. Analysis of the same step using the water H_2O (Wat1) as a nucleophile was also carried out, which suggests this mechanistic scenario to be energetically demanding (see **Figure S4**). Figure 3 shows the optimized structures of transition states, intermediates and product obtained for this path. The critical C1-O_μ distance is 1.91 Å at **TS1-A** and is fully bonded at **IM1-A** with a bond distance of 1.51 Å. The corresponding **TS1-A** has an imaginary frequency of 190*i* cm^{-1}. The barrier of this step is calculated to be 6.3 kcal/mol (7.2 kcal/mol without solvation) and the energy of **IM1-A** is calculated to be 5.3 kcal/mol (7.5 kcal/mol without solvation) relative to the **R-A**. The hydroxyl group of the gem-diolate forms a hydrogen bond to His178 with a Nε-H_μ distance of 1.63 Å, setting a stage for further proton transfer assisted by His178. The shortening of the Nε-H_μ distance (from 1.87 Å in **R-A** to 1.63 Å in **IM1-A)**, and the Zn1-O_α distance (from 2.10 Å in **R-A** to 1.87 Å in **IM1-A)** implies that His178 and Zn1 anticipate in stabilizing the transition state and tetrahedral intermediate, thereby lowering the barrier for the nucleophilic attack. During this step, the coordination number (CN) of Zn1 changes from 5 to 4, resulting from the detachment of O_μ from Zn1 (2.03 Å at **R-A** to 2.96 Å at **IM1-A**), while the tetracoordination geometry of Zn2 remains unaltered (CN = 4). This also explains the laboratory experiment why Zn1 can be replaced by other divalent cations such as Mn^{2+} or Co^{2+} [41].

The next step (**IM1-A→P-A**) is the ring opening which involved the proton transfer and the C1-N1 bond cleavage, assisted by the His178 residue. As suggested by previous studies [11, 15], His178 now plays a central role by shuttling a proton from the hydroxide of gem-diolate intermediate to the nitrogen leaving group of the creatinine ring. From the QM-cluster calculations, this process appears to occur as two separate steps, consisting of His178 protonation and subsequent C1-N1 bond fission (via two transition states **TS2-A** and **TS3-A**). At **TS2-A**, the transferring proton (H_μ) is in between the Nε atom of His178 imidazole ring and the gem-diolate O_μ atom (Nε-H_μ = 1.43 Å, O_μ-H_μ = 1.48 Å; **TS2-A** in Fig. 3) and this corresponds to the stretching of the Nε-H_μ and O_μ-H_μ bonds as evident by the imaginary value of 1691*i* cm^{-1}. After **TS2-A**, His178 is now fully protonated (Nε-H_μ = 1.08 Å) and, by orienting its imidazole ring, forms a hydrogen bond to the nitrogen leaving group (N1-H_μ = 1.63 Å at **IM2-A**). At **IM2-A**, due to the loss of one proton to His178, the bridging hydroxyl is now ionized and unstable, which is then stabilized by coordinating with Zn1 as a fifth ligand (CN = 5 at Zn1). This Zn1 remains pentacoordinated until the formation of the product state, where Wat2 is ligated as a sixth ligand in a hexacoordination sphere. The **TS3-A** structure, as confirmed by one imaginary value of 1355*i* cm^{-1}, shows that the transferring proton is approximately in half way between the Nε(His178) and the nitrogen leaving group (Nε-H_μ = 1.31 Å; N1-H_μ = 1.39 Å). Downhill from **TS3-A**, the H_μ proton is completely transferred to the C1-N1 amide bond (N1-H_μ = 1.03 Å), which is subsequently breaks (C1-N1 = 2.06 Å) to yield a product creatine with C-terminal carboxylate bound in the dizinc site in a bidentate fashion. The barriers of this ring-opening step were 19.8 kcal/mol (24.0 kcal/mol without solvation) for the His178 protonation and 11.6 kcal/mol (14.0 kcal/mol without solvation) for the C1-N1 bond cleavage, indicating the first proton transfer by His178 is the rate-limiting step. The overall reaction is slightly exothermic by -5.4 kcal/mol (-4.9 kcal/mol without solvation). Note that the role of the proton shuttle His178 was also seen in other amino acid residues of both mono- and dizinc metalloenzymes (e.g., Asp250 in dihydroorotase [17], Asp288 in human renal peptidase [18], Glu384 of human angiotensin-converting enzyme [37], His216 of the β-carbonic anhydrase [42]).

Path B1

The proposed mechanism in path A suggests that the His178 residue plays the key roles during catalysis: its serves as an electrostatic stabilizer in the nucleophilic attack and a proton shuttle in the ring-opening step. However, a water molecule that situates very close to Zn1 and hydrogen bonds with Glu34 and Glu122 (Glu34-Wat2-Glu122 partner) might serve as a proton donor in the ring-opening, as suggested by Yoshimoto et al. [13, 14]. Figure 4 shows the optimized

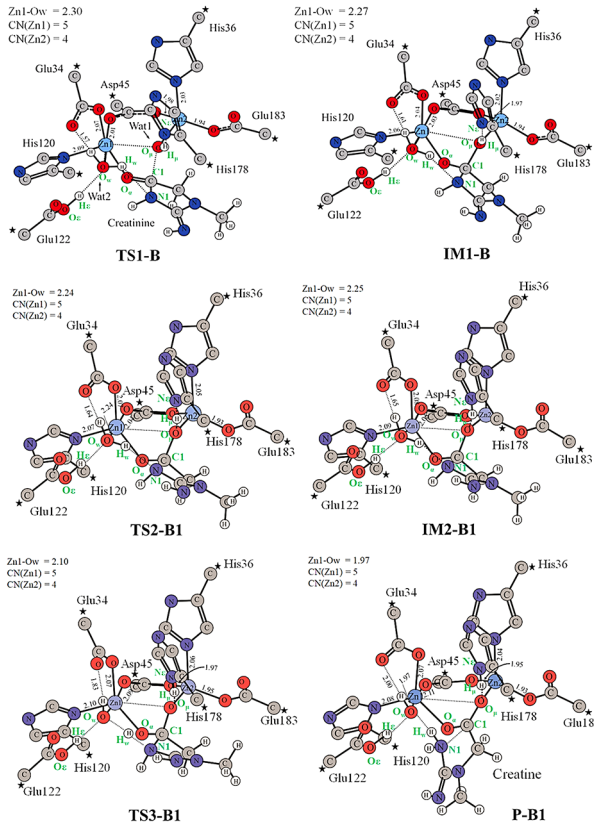

Fig. 4 DFT optimized structures of transition states, intermediates and product for path B1. The fixed atoms are marked with asterisks. Distances are in angstrom (Å)

transition states, intermediates and product for the nucleophilic attack and ring-opening of path B2. As in the first step of path A, the nucleophilic attack readily takes place from a bridging position, and the C1-O_μ distance decreases from 2.49 Å at **R-B** to 1.79 Å at **TS1-B**, and further to 1.49 Å at **IM1-B**. This **TS1-B** exhibits an imaginary value of $245icm^{-1}$. The resulting intermediate **IM1-B** lies 11.9 kcal/mol higher than **R-B**. Despite the fact that the transition state structure **TS1-B** is quite similar to that of **TS1-A**, however, the barrier is calculated to be 13.6 kcal/mol (11.6 kcal/mol without solvation), which is two-fold higher than the corresponding barrier (6.3 kcal/mol) of path A. The reason for the higher barrier at **TS1-B** may be explained by the higher coordination number (CN) at Zn1 in path B (CN = 5), compared with that of path A (CN = 4). The lower **TS1-A** barrier compared to the corresponding **TS1-B** might be explained from the better nucleophile and electrophile of $O_\mu H_\mu^-$ and C1 atom, as evident from the more negative and positive charge on them (O_μ = -0.81*e* to -0.95*e* and C1 = + 0.62*e* for path A vs. O_μ = -0.78*e* to -0.96*e* and C1 = + 0.60*e* for path B, **Table S2**). From **TS1-B→IM1-B**, Wat2 is now fully coordinated to Zn1 (Zn1-O_α = 2.30 and 2.27 Å, respectively), which is not present in path A (Zn1-O_α > 3.5 Å) and the previous free-energy simulations [15]. At **IM1-B**, after Zn1 coordination rearrangement, Wat2 now serves as the fifth ligand of Zn1 and, as stabilized by Glu34 and Glu122 via two hydrogen bonds (1.61 and 1.68 Å, respectively), is allowed to orient its position to form a hydrogen bond (2.02 Å at **IM1-B**) to the N1 atom of creatinine, which is distorted away from the planar ring (see **IM1-B**, Fig. 4). Conversely, this amide bond is directly hydrogen bonding with the oxygen atom (O_w) of Wat2 in path A. This process is required for next proton transfer step.

The ring-opening step in this pathway basically followed the same mechanism as in path A, i.e., the protonation of His178 and the breaking of the scissile bond. In this scenario, it is not His178 that plays this role as a central catalyst. On the other hand, it is also envisioned that both His178 and Wat2 might play a catalytic role as base and acid, respectively. In this path B1, the protonated His178 intermediate (**IM1-B→ IM2-B1**) is formed, as evident from the shortening of the N_ε-H_μ distance from 1.76 Å to 1.00 Å, respectively. At **TS2-B**, the critical bonds, O_μ-H_μ and N1-H_μ, are 1.40 and 1.34 Å, respectively, with one imaginary frequency ($1546i\ cm^{-1}$). During this stage, the substrate amide bond is more distorted due to the shortened H_w-N1 distance from 2.02 Å at **IM1-B** to 1.80 Å at **IM2-B2**. This structural arrangement prompts further proton transfer in the protonation of substrate amide bond that leads to the ring-opening. In **IM2-B→ P-B1**, the protonation of the substrate by Wat2 results in the elongation of C1-N1 bond (1.50 Å at **IM2-B1** to 3.43 Å at **P-B1**) and the breakdown of creatinine ring into creatine product. The two critical distances, O_w-H_w and N1-H_w, of this process are 1.42 and 1.35 Å at **TS3-B**, yielding one imaginary number ($1488i\ cm^{-1}$) corresponding to the stretching of these bonds. At the end of this process, a penta-coordinated complex is obtained.

Path B2

The two proposed mechanisms above suggest that the reaction proceeds via the protonated His178 before the C1-N1 bond cleavage and ring-opening assisted by a proton donor (His178 in path A or Wat2 in path B1). In fact, a water molecule that situated very close to Zn1 might play this role during the course of the reaction, as suggested by Yoshimoto et al. [13], without the His178 protonation as described earlier. In particular, we also tested another pathway where Wat2 serves as the catalytic acid and His178 maintains its neutral form during the catalysis. Figure 5 shows the optimized transition states, intermediates and product for this path. Since the nucleophilic attack follows the same pathway as in the case of path B1, therefore we will discuss only the second ring-opening step.

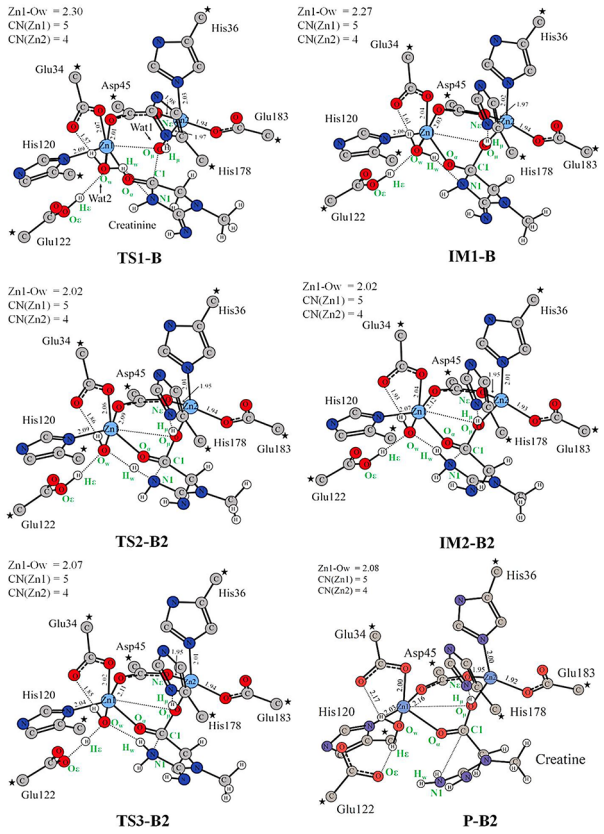

Fig. 5 DFT optimized structures of transition states, intermediates and product for path B2. The fixed atoms are marked with asterisks. Distances are in angstrom (Å)

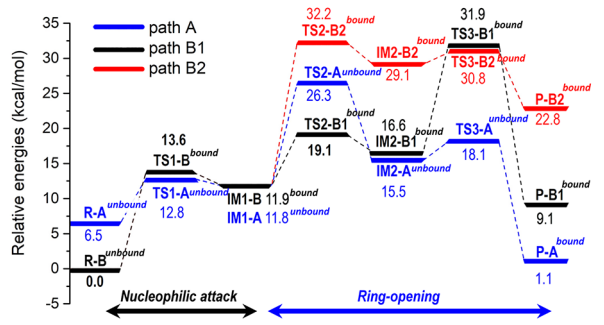

Fig. 6 Relative potential energy profiles of the creatinine hydrolysis for paths A, B1, and B2. The *bound* and *unbound* modes of Wat2 at Zn1 are also indicated

In the ring-opening step, the tetrahedral intermediate is subsequently collapsed by the donation of a proton (H_w) from Wat2 to the amide of the substrate (**IM1-B→IM2-B2**), followed by the transfer of a proton (H_ε) from Glu122 to Wat2 to regenerate a water molecule (**IM2-B2→P-B2**). The critical bond distances for the first proton transfer are calculated at 1.60 (O_w-H_w) and 1.22 (N1-H_w) Å at **TS2-B2**. Meanwhile, the transient bonds for the second proton transfer by Glu122 are 1.39 (O_ε-H_ε) and 1.28 (O_w-H_ε) Å at **TS3-B2**. Values of imaginary frequency of these two transition states (**TS2-B2** and **TS3-B2**) are 827*i* and 1351*i* cm^{-1}, respectively. The barriers of these proton transfers are 32.2 at **TS2-B2** and 30.8 kcal/mol at **TS3-B2**, which is much higher than the other pathways. This clearly indicates that the proton transfer from Wat2 to the scissile bond of substrate is very unfeasible when His178 is neutral and this renders ineffective catalysis. However, His178 still provides stabilization to the reaction via hydrogen bonding to the gem-diolate hydroxide, as can be seen from the decreasing of N_ε-H_μ distances (1.95, 1.76, 1.69, 1.68, 1.68 and 1.41 Å at **TS1-B, IM1-B**, **TS2-B2**, **IM2-B2**, **TS3-B2**, **P-B2**, respectively). The C1–N1 distance of 3.15 Å at **P-B2** clearly indicates that the amide bond of the creatinine ring is fully broken, yielding the creatine product with the amine and carboxylic groups. These stepwise proton transfers lead to the cleavage of the amide bond of the substrate releasing a creatine molecule.

Summary

In general, the first nucleophilic attack for all pathways (A, B1 and B2) is the same, i.e. the attack of hydroxide on the substrate carbonyl that leads to the formation of tetrahedral gem-diolate intermediate (see **IM1-A** in Fig. 2 and **IM1-B** in Figs. 4 and 5). However, in the second ring-opening step, the proton donor can be either His178 or Wat2 (see Scheme 1) or both, which delivers its proton to the substrate for opening the creatinine ring to yield the creatine product. In the ring opening of path A, His178 serves as a proton shuttle by accepting one proton of the -OH group of the gem-diolate intermediate (and His178 is now protonated; see *His178 protonation* step in Scheme 1) and transferring it to the substrate. During this step, Wat2 is unbound at Zn1 and does not participate during catalysis. In the ring opening of path B1, His178 is protonated via the same pathway as in path A but the cleavage of the substrate ring is now activated by the proton transfer from Wat2, which turn into a hydroxide at the final product. Alternatively, in path B2, His178 is unprotonated and the proton transfer from Wat2 to the substrate is assisted by Glu122.

Comparison of energetic profiles for all possible pathways in Fig. 1 also shows that the enzyme likely favors the pathway involved in the protonation of His178 (paths A and B1) prior to the ring cleavage. In path A, His178 acts as a catalytic base/acid, and in path B1 His178 and Wat2 can serve as an equal foot as the catalytic base and the catalytic acid, respectively. Alternatively, Wat2 might function as the catalytic acid in assisting ring-opening pathway (path B2).

Table 1 Values of important structural parameters (distances in Å) of the optimized reactant, intermediates, transition states, and product in paths A, B1 and B2 for the hydrolysis of dizinc creatininase

	R-A	TS1-A	IM1-A	TS2-A	IM2-A	TS3-A	P-A	Exp[a]
Zn1–Zn2	3.40	3.40	3.88	3.75	3.61	3.63	3.89	3.56
Zn1–Ow	3.81	3.56	3.70	3.77	3.70	3.66	2.16	2.28
Zn1–Oμ	2.04	2.32	2.98	2.80	2.30	2.30	2.41	2.27
Zn2–Oμ	1.94	1.94	2.00	1.95	1.91	1.91	1.97	1.94
C1–Oμ	2.51	1.91	1.52	1.45	1.40	1.38	1.28	1.26
C1–Oα	1.24	1.28	1.34	1.36	1.36	1.35	1.25	1.25
C1–N1	1.35	1.37	1.44	1.46	1.51	1.55	2.95	2.67
Zn1–Oα	2.10	1.96	1.87	1.87	1.91	1.93	2.16	2.38
O_{μ}-H_{μ}	1.08	0.99	1.08	1.48	2.28	2.34	3.01	-
Nε-H_{μ}	1.87	1.99	1.63	1.43	1.08	1.31	2.17	-
N1-H_{μ}	2.91	2.56	2.29	2.32s	1.63	1.39	1.03	-
	R-B	**TS1-B**	**IM1-B**	**TS2-B1**	**IM2-B1**	**TS3-B1**	**P-B1**	
Zn1–Zn2	3.32	3.69	3.86	3.73	3.61	3.61	3.96	
Zn1–Ow	3.22	2.31	2.27	2.25	2.26	2.11	1.98	
Zn1–Oμ	1.98	2.49	2.93	2.90	2.81	2.79	3.21	
Zn2–Oμ	1.96	1.98	2.00	1.96	1.94	1.96	2.00	
C1–Oμ	2.49	1.79	1.49	1.43	1.40	1.40	1.31	
C1–Oα	1.23	1.28	1.32	1.34	1.34	1.33	1.24	
C1–N1	1.36	1.42	1.50	1.52	1.55	1.55	3.43	
Zn1–Oα	2.39	2.01	1.95	1.94	1.93	2.01	2.16	
O_{μ}-H_{μ}	0.98	0.98	1.00	1.40	1.67	1.76	1.68	
Nε-H_{μ}	1.99	1.95	1.76	1.34	0.99	1.00	0.99	
	R-B	**TS1-B**	**IM1-B**	**TS2-B2**	**IM2-B2**	**TS3-B2**	**P-B2**	
Zn1–Zn2	3.32	3.69	3.86	3.82	3.93	4.01	4.30	
Zn1–Ow	3.22	2.31	2.27	2.02	2.02	2.07	2.08	
Zn1–Oμ	1.98	2.49	2.93	3.09	3.01	3.23	3.36	
Zn2–Oμ	1.96	1.98	2.00	2.04	2.05	2.07	2.12	
C1–Oμ	2.49	1.79	1.49	1.46	1.45	1.44	1.34	
C1–Oα	1.23	1.28	1.32	1.29	1.28	1.27	1.22	
C1–N1	1.36	1.42	1.50	1.59	1.64	1.70	3.16	
Zn1–Oα	2.39	2.01	1.95	2.09	2.10	2.07	2.18	
O_w-H_w	0.97	0.97	0.98	1.60	1.90	1.96	3.07	
N1-H_w	3.01	2.46	2.02	1.22	1.02	1.04	0.98	
O_w-H_{ε}	1.80	1.77	1.68	1.68	1.60	1.28	1.03	
O_{ε}-H_{ε}	0.99	0.99	1.00	1.00	1.00	1.39	1.57	

[a] Taken from PDB entry 1V7Z

However, due to the high-energy pathway, this mechanistic scenario is not very likely.

Can Wat2 ligand exchange at Zn1 lead to different catalytic route?

From Fig. 6, it is clear that path A gives quite feasible barrier (19.8 kcal/mol) for the creatinine hydrolysis. The calculated energetics of path A described above agrees well with the available experimental kinetics (k_{cat} = 252 s^{-1} [13] which can be converted to a barrier of ~ 14.1 kcal/mol according to transition state theory). It is also in line with the recent QM/MM study [15]. However, our QM study suggests one more step is needed in the ring-opening step starting from **IM1-A**.

It can be seen from Fig. 6 that, for path A, the highest barrier of 26.3 kcal/mol (19.8 kcal/mol relative to **R-A**) is found at **TS2-A** for His178 protonation (**IM1-A**→ **IM2-A**) while the proton transfer from His178 to substrate (**IM2-B1** → **P-B1**) is the rate-limiting step for path B1 (**TS3-B1** = 31.9 and 25.4 kcal/mol, relative to **R-B** and **R-A**, respectively). Both path A and B1 share the same intermediate species at **IM2**, which involves a protonated His178 residue. The two species, **IM2-A** and **IM2-B**, have similar energies on the potential energy surface (15.5 vs. 16.6 kcal/mol, Fig. 6). Analysis of relative energies of these pathways using different DFT functional and a bigger basis set (6-311 + G(2d,2p)) was also carried out and it shows that these two geometries have a close energy (18.5 ± 2.7 kcal/mol for **IM2-A** and 20.0 ± 2.6 kcal/mol **IM2-B1**, **Table S3** and **Figure S5**). The

main difference between **IM2-A** and **IM2-B1** is the geometrical rearrangement of Wat1 and Wat2 with respect to Zn1, via Oμ and O_w atoms, respectively (Zn1-Oμ = 2.30 Å, Zn1-Ow = 3.70 Å for **IM2-A** and Zn1-Oμ = 2.81 Å, Zn1-Ow = 2.26 Å for **IM2-B1**), as shown in Fig. 7. These data also reflect that this arrangement is necessary to keep Zn1 in a penta-coordination fashion. Hydrogen bond interactions also play an important role and they are found in both structures where Glu122 and Glu34 participate in stabilizing the Wat2. His178, on the other hand, shows different H-bond interactions between the -NH group of His178 and the substrate.

Considering the close energy for two different Zn1 coordination geometries at **IM2-B1** and **IM2-A**, it could be envisioned that another alternative pathway could also be possible, i.e., bound (**R-B** → **TS1-B** → **IM1-B** → **TS2-B1**) → unbound (**IM2-A** → **TS3-A**) → bound (**P-A**). This alternative pathway has similar barriers of 19.1 and 18.1 kcal/mol at **TS2-B1**^{bound} and **TS3-A**^{unbound}, respectively, which indicates that the two mechanistic steps in the ring-opening, occurs sequentially with comparable rates. Such a route was not suggested by our previous QM/MM simulations, possibly due to the weak coordination of Wat2 at Zn1 during the course of reaction [15].

Now, we look further into the change of coordination number at Zn1 and Zn2. As depicted in Fig. 8, during the ring-opening step of path B1 and B2, the 5-fold coordination is maintained at Zn1, while the 4-fold coordination in Zn2. However, for the same step in path A, there is an increasing of Zn1 coordination number from 4 to 6 at **IM1-A**, **IM2-A** and **P-A**, respectively. There is a good correlation between the Zn1 coordination with oxygen atom of Wat2 (O_w) and oxygen atom (O_μ) of substrate in path A (see distances Zn1-O_{Wat2} and Zn1-O_μ in **Figure S6**). Meanwhile, path B1 and B2 show a good correlation between the O_w and oxygen atom (O_μ) of hydroxide (Wat1). These results also implied that the fast ligand exchange at Zn1 can lead to different coordination modes that yield different several energetically favorable pathways, as described by Brás et al. [37].

Overall, this DFT cluster approach not only allows us to examine reaction pathways of this enzyme but also provide important insights into key intermediate species of the ring-opening step, which was found to occur via a stepwise mechanism assisted by His178 (a proton transfer takes places from the bridging hydroxyl group to His178, couple with a rotation of the latter to form a hydrogen bond to the substrate amide nitrogen, which becomes ready for protonation). In other word, the protonation of His178 and the C1-N1 bond cleavage occurs via two transition states (via **TS2** and **TS3**). In the previous QM/MM study, the proton transfer from the bridging hydroxyl group to the amide nitrogen proceeds in a single concerted step.

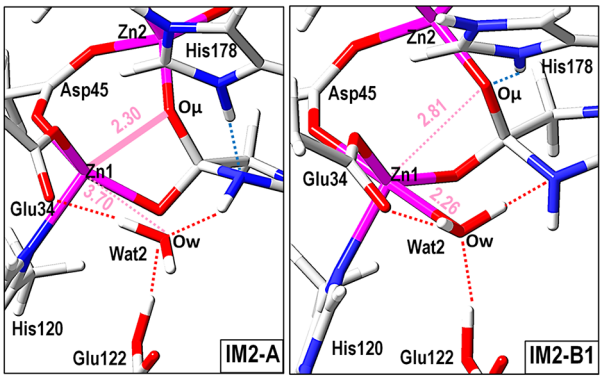

Fig. 7 Comparison of structures IM2-A and IM2-B1. Hydrogen bonds originated from Wat2 and His178 were depicted as dotted lines with red and blue colors, respectively. Zn1 coordination distances with Oμ (Wat1) and Ow atoms (Wat2) were also indicated. Distances are in angstrom (Å)

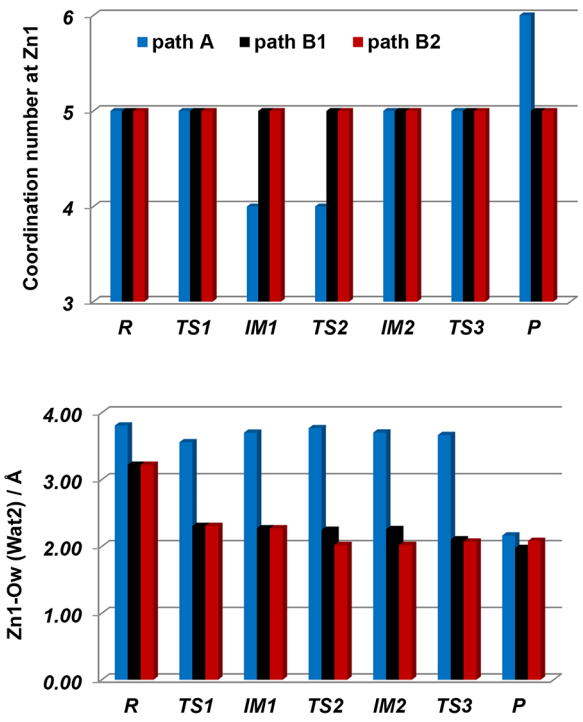

Fig. 8 Bar graph showing the changes of coordination number at Zn1 (top) and Zn1-O_w(Wat2) distance (bottom) for paths A, B1, and B2, shown in blue, black and red, respectively. The criteria for the *bound* and *unbound* geometries of Wat2 at Zn1 were measured by the Zn1-O_w distance, having a cut-off of < 3.00 Å and > 3.00 Å, respectively

The influence of different functional and basis set

In order to assess the influence of functional on the reaction of creatininase, several different functional (B3LYP, B3LYP-D3, X3LYP, B97-D, B97-2, B1B95, mPWB1K, M06-L, M06-2X, M05-2) were performed using the single-point energy calculations with the larger basis set (6-311 + G(2d,2p) (**Table S3** and **Figure S5**). As results, the lowest activation barriers of 22.1 ± 2.4 kcal/mol were obtained for path A, while paths B1 and B2 yielded very large barriers at **TS3** (37.2 ± 2.8 and 37.6 ± 2.3 kcal/mol). These results clearly indicate that path A is the likely mechanism of creatininase, with the proximate energy value to experimental value. Therefore, using different functional and a larger basis set (6-311 + G(2d,2p)) do not change significantly the results drawn above and the calculations discussed in the main text are still valid.

Conclusions

In the present work, the catalytic mechanism of creatininase-catalyzed reaction has been investigated by DFT cluster approach. Three reaction pathways (paths A, B1 and B2, Scheme 1) were modeled using the X-ray crystal structure of the product-bound enzyme as a starting point of the current investigation. It is shown that the reaction mechanism shown in Scheme 1 (corresponding to path A) is energetically more feasible and is in agreement with available experimental kinetic (14.1 kcal/mol derived from k_{cat} of 252 s^{-1} [13]) and our recent QM/MM study [15]. Owing to fast exchange of Wat2 ligand at Zn1, an alternative/competitive ring-opening pathway to path A (via **TS2-B1** and **TS3-A**) can occur with His178 and Wat2 serving as a dual role as the catalytic base and the catalytic acid, respectively. The overall mechanism of the creatininase is proposed to follow three elementary steps: nucleophilic attack by the bridging hydroxide. Collapse of the tetrahedral intermediate and cleavage of the C1-N1 bond occur via a sequence of two proton transfer steps with the assistance of His178 or Wat2: the abstraction of a proton from the gem-diolate tetrahedral intermediate by His178 followed by the proton transfer from this protonated histidine to the amide of substrate, resulting in the formation of creatine product. The first proton transfer is the rate-limiting step with the computed barrier of ~ 19 kcal/mol. Calculations have also confirmed that His178 plays a crucial role in stabilizing the transition state and intermediate during catalysis. The detailed mechanistic understanding in this study might be extended to other members of the cyclic amidohydrolase family and may facilitate future rational design of enzymes for biosensor application.

Supplementary Information The online version contains supplementary material available at https://doi.org/10.1007/s10822-022-00451-8.

Acknowledgements Financial supports by the Thailand Research Fund and the University of Phayao (Grants RSA6280104 and FF64-RIB002) are gratefully acknowledged. The School of Science, University of Phayao (Grant PBTSC65006) is also acknowledged. The authors acknowledge National e-Science Infrastructure Consortium for providing computing resources that have partly contributed to the research results reported within this paper (www.e-science.in.th).

Data Availability All data generated or analysed during this study are included in this published article (and its supplementary information files).

References

1. Szulmajster J (1958) Bacterial degradation of creatinine. II. Creatinine desimidase. Biochim Biophys Acta 30(1):154
2. Wyss M, Kaddurah-Daouk R (2000) Creatine and creatinine metabolism. Physiol Rev 80(3):1107
3. Kaplan A, Szabo LL (1974) Creatinine hydrolase and creatine amidinohydrolase. II. Partial purification and properties. Mol Cell Biochem 3:17
4. Tsuru D, Oka I, Yoshimoto T (1976) Creatinine decomposing enzymes in Pseudomonas putida. Agric Biol Chem 40:1011
5. Rikitake K, Oka I, Ando M, Yoshimoto T, Tsuru D (1979) Creatinine amidohydrolase (creatininase) from Pseudomonas putida. Purification and some properties. J Biochem 86:1109
6. Tang TY, Wen CJ (2000) Expression of the creatininase gene from Pseudomonas putida RS65 in Escherichia coli. J Ind Microbiol 24:2
7. Yoshimoto T, Oka I, Tsuru D (1976) Creatine amidinohydrolase of Pseudomonas putida: Crystallization and some properties. Arch Biochem Biophys 177(2):508
8. Schumann J, Böhm G, Schumacher G, Rudolph R, Jaenicke R (1993) Stabilization of creatinase from Pseudomonas putida by random mutagenesis. Protein Sci 2(10):1612
9. Yamamoto K, Oka M (1995) Cloning of the creatinine amidohydrolase gene from Pseudomonas sp. PS-7. Biosci Biotechnol Biochem 59:1331
10. Beuth B, Niefind K, Schomburg D (2002) Crystallization and preliminary crystallographic analysis of creatininase from Pseudomonas putida. Acta Crystallogr D Biol Crystallogr 58(8):1356
11. Beuth B, Niefind K, Schomburg D (2003) Crystal structure of creatininase from Pseudomonas putida: a novel fold and a case of convergent evolution. J Mol Biol 332(1):287
12. Ito K, Kanada N, Inoue T, Furukawa K, Yamashita K, Tanaka N, Nakamura KT, Nishiya Y, Sogabe A, Yoshimoto T (2002) Preliminary crystallographic studies of the creatinine amidohydrolase from Pseudomonas putida. Acta Crystallogr Sect D 58:2180
13. Yamashita K, Nakajima Y, Matsushita H, Nishiya Y, Yamazawa R, Wu YF, Matsubara F, Oyama H, Ito K, Yoshimoto T (2010) Substitution of Glu122 by glutamine revealed the function of the second water molecule as a proton donor in the binuclear metal enzyme creatininase. J Mol Biol 396(4):1081
14. Yoshimoto T, Tanaka N, Kanada N, Inoue T, Nakajima Y, Haratake M, Nakamura KT, Xu Y, Ito K (2004) Crystal structures of creatininase reveal the substrate binding site and provide an insight into the catalytic mechanism. J Mol Biol 337(2):399
15. Jitonnom J, Mujika JI, van der Kamp MW, Mulholland AJ (2017) Quantum mechanics/molecular mechanics simulations

identify the ring-opening mechanism of creatininase. Biochemistry 56(48):6377
16. Seibert CM, Raushel FM (2005) Structural and catalytic diversity within the amidohydrolase superfamily. Biochemistry 44(17):6383
17. Liao R-Z, Yu J-G, Frank M, Raushel, Himo F (2008) Theoretical investigation of the reaction mechanism of the dinuclear zinc enzyme dihydroorotase. Chem Eur J 14:4287
18. Liao R-Z, Himo F, Yu J-G, Liu R-Z (2010) Dipeptide hydrolysis by the dinuclear zinc enzyme human renal dipeptidase: Mechanistic insights from DFT calculations. J Inorg Biochem 104(1):37
19. Liao R-Z, Yu J-G, Himo F (2009) Reaction Mechanism of the Dinuclear Zinc Enzyme N-Acyl-l-homoserine Lactone Hydrolase: A Quantum Chemical Study. Inorg Chem 48(4):1442
20. Krivitskaya AV, Khrenova MG, Nemukhin AV (2021) Two Sides of Quantum-Based Modeling of Enzyme-Catalyzed Reactions: Mechanistic and Electronic Structure Aspects of the Hydrolysis by Glutamate Carboxypeptidase. Molecules 26(20):6280
21. Reidl CT, Mascarenhas R, Mohammad TSH, Lutz MR Jr, Thomas PW, Fast W, Liu D, Becker DP (2021) Cyclobutanone Inhibitor of Cobalt-Functionalized Metallo-γ-Lactonase AiiA with Cyclobutanone Ring Opening in the Active Site. ACS omega 6(21):13567
22. Liao R-Z, Yu J-G, Himo F (2010) Reaction Mechanism of the Trinuclear Zinc Enzyme Phospholipase C: A Density Functional Theory Study. J Phys Chem B 114(7):2533
23. Zhu X, Barman A, Ozbil M, Zhang T, Li S, Prabhakar R (2012) Mechanism of peptide hydrolysis by co-catalytic metal centers containing leucine aminopeptidase enzyme: a DFT approach. J Biol Inorg Chem 17(2):209
24. Manta B, Raushel FM, Himo F (2014) Reaction mechanism of zinc-dependent cytosine deaminase from Escherichia coli: a quantum-chemical study. J Phys Chem B 118(21):5644
25. Jitonnom J, Sattayanon C, Kungwan N, Hannongbua S (2015) A DFT study of the unusual substrate-assisted mechanism of Serratia marcescens chitinase B reveals the role of solvent and mutational effect on catalysis. J Mol Graph Model 56:53
26. Jitonnom J, Hannongbua S (2018) Theoretical study of the arabinan hydrolysis by an inverting GH43 arabinanase. Mol Simul 44(8):631
27. Fernandes HS, Teixeira CSS, Sousa SF, Cerqueira NMFSA (2019) Formation of unstable and very reactive chemical species catalyzed by metalloenzymes: a mechanistic overview. Molecules24(13)
28. Jitonnom J, Lee VS, Nimmanpipug P, Rowlands HA, Mulholland AJ (2011) Quantum mechanics/molecular mechanics modeling of substrate-assisted catalysis in family 18 chitinases: conformational changes and the role of Asp142 in catalysis in ChiB. Biochemistry 50(21):4697
29. Himo F (2017) Recent Trends in Quantum Chemical Modeling of Enzymatic Reactions. J Am Chem Soc 139(20):6780
30. Siegbahn PEM, Himo F (2011) The quantum chemical cluster approach for modeling enzyme reactions. Wiley Interdisciplinary Reviews: Computational Molecular Science 1(3):323
31. Siegbahn PE, Himo F (2009) Recent developments of the quantum chemical cluster approach for modeling enzyme reactions. J Biol Inorg Chem 14(5):643
32. Ahmadi S, Barrios Herrera L, Chehelamirani M, Hostaš J, Jalife S, Salahub DR (2018) Multiscale modeling of enzymes: QM-cluster, QM/MM, and QM/MM/MD: A tutorial review. Int J Quantum Chem 118(9):e25558
33. Mulliken RS (1955) Electronic population analysis on LCAO–MO molecular wave functions. I J Chem Phys 23(10):1833
34. Cossi M, Rega N, Scalmani G, Barone V (2003) Energies, structures, and electronic properties of molecules in solution with the C-PCM solvation model. J Comput Chem 24(6):669
35. Grimme S, Antony J, Ehrlich S, Krieg H (2010) A consistent and accurate ab initio parametrization of density functional dispersion correction (DFT-D) for the 94 elements H-Pu. J Chem Phys 132(15):154104
36. Grimme S, Ehrlich S, Goerigk L (2011) Effect of the damping function in dispersion corrected density functional theory. J Comput Chem 32(7):1456
37. Brás NF, Fernandes PA, Ramos MJ (2014) QM/MM study and MD simulations on the hypertension regulator angiotensin-converting enzyme. ACS Catal 4(8):2587
38. Lonsdale R, Harvey JN, Mulholland AJ (2010) Inclusion of dispersion effects significantly improves accuracy of calculated reaction barriers for cytochrome P450 catalyzed reactions. J Phys Chem Lett 1(21):3232
39. Lonsdale R, Harvey JN, Mulholland AJ (2012) Effects of dispersion in density functional based quantum mechanical/molecular mechanical calculations on cytochrome P450 catalyzed reactions. J Chem Theory Comput 8(11):4637
40. Frisch MJ, Trucks GW, Schlegel HB, Scuseria GE, Robb MA, Cheeseman JR, Scalmani G, Barone V, Petersson GA, Nakatsuji H, Li X, Caricato M, Marenich AV, Bloino J, Janesko BG, Gomperts R, Mennucci B, Hratchian HP, Ortiz JV, Izmaylov AF, Sonnenberg JL, Williams, Ding F, Lipparini F, Egidi F, Goings J, Peng B, Petrone A, Henderson T, Ranasinghe D, Zakrzewski VG, Gao J, Rega N, Zheng G, Liang W, Hada M, Ehara M, Toyota K, Fukuda R, Hasegawa J, Ishida M, Nakajima T, Honda Y, Kitao O, Nakai H, Vreven T, Throssell K, Montgomery JA Jr, Peralta JE, Ogliaro F, Bearpark MJ, Heyd JJ, Brothers EN, Kudin KN, Staroverov VN, Keith TA, Kobayashi R, Normand J, Raghavachari K, Rendell AP, Burant JC, Iyengar SS, Tomasi J, Cossi M, Millam JM, Klene M, Adamo C, Cammi R, Ochterski JW, Martin RL, Morokuma K, Farkas O, Foresman JB, Fox DJ (2009) Gaussian 09 Rev. A.02. Wallingford, CT;
41. Kim H, Lipscomb WN (1993) Differentiation and identification of the two catalytic metal binding sites in bovine lens leucine aminopeptidase by x-ray crystallography. Proc Natl Acad Sci USA 90(11):5006
42. Rowlett RS, Tu C, McKay MM, Preiss JR, Loomis RJ, Hicks KA, Marchione RJ, Strong JA, Donovan GS Jr, Chamberlin JE (2002) Kinetic characterization of wild-type and proton transfer-impaired variants of beta-carbonic anhydrase from Arabidopsis thaliana. Arch Biochem Biophys 404(2):197